PLASMA ENERGETICS IN SOLAR FLARES

Gerard Van Hoven
Department of Physics; University of California;
Irvine, California 92717

I want to begin with the observation, which I will try to make clear in the following, that a solar flare comprises an incredibly complex set of phenomena. This is not only true with respect to what is seen and measured in spectacular examples, but also when one considers the constituent parts of simple, even idealized, cases. A series of different physical effects lead, as one illustration, to radiations from the flare-instability site and its surroundings which span the range from meter waves to gamma rays (Svestka 1976, Sturrock 1979).

To fit within the context of this discussion, I will concentrate on the high-temperature and quasi-thermal aspects of a flare, and on the basic physical mechanisms connected with the primary energization and dissipation processes. Thus, I will treat the reconnection of the magnetic field, the bulk acceleration of particles, the thermalization and the ultimate radiation of the energy. I will not treat the optical manifestations or, at the other extreme, the acceleration of very high energy particles.

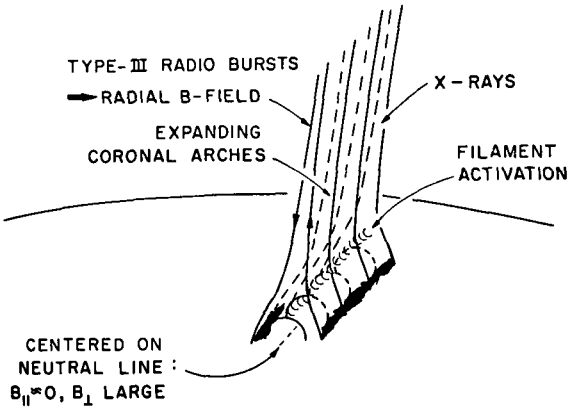

Fig. 1. The Magnetic Field and some Outputs of a Two-Ribbon Flare.

Solar flares occur in two principal magnetic configurations. Figure 1 shows the preflare magnetic structure of the classic large-scale two-ribbon variety, along with some of the observable consequences. In this review, I will emphasize the effects occurring in the hot diffuse corona ($n_e \sim 10^9 cm^{-3}$ and $T_e \sim 10^{6.3} K$, shown above) and only the high temperature manifestations of the fall-out onto the solar surface ($n_e > 10^{12}$, $T_e < 10^4$).

Patrick A. Wayman (ed.), Highlights of Astronomy, Vol. 5, 343–350.

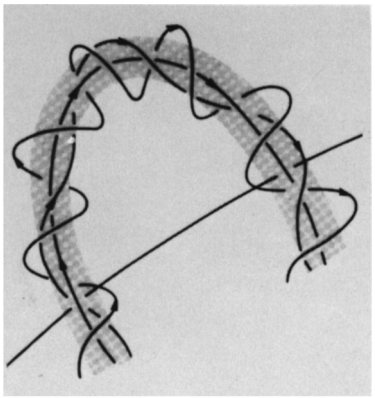

Fig. 2.
The Field of a Loop Flare.

It should be mentioned, however, that the preflare state is definitely not isothermal, and significant effects occur in connection with cool inclusions of plasma (such as the 10^4 K filament shown) at the flare site (Van Hoven et al. 1979). Figure 2 shows the ambient magnetic field collimating the alternative case of a smaller simple-loop flare (as prominently observed by the Skylab instruments) including, once again, cool material along the axis.

Most important in both of these situations is the influence of the magnetic field which, by common agreement, provides both the energy supply (10^{29} - 10^{32} ergs) for the flare and the confinement ($B \sim 10^2$G) of its structure (Van Hoven et al. 1979).

A second crucial aspect of each of these examples is the existence of shear in the magnetic fields, due to the flow of current in the corona. One consequently has an excess of stored energy, above the potential (or current-free) state. An important question is how can this energy be released into the solar environment? First, one requires a change in the field topology, so that it is free to relax, and this indicates the influence of finite plasma resistivity (Van Hoven 1976, 1979). If one considers the actual temperatures and sizes, however, one can see that simple resistive diffusion (τ_r) is much too slow. What is needed is an intermediate mechanism, anomalous in the terms of normal infinite-conductivity magnetohydrodynamics (MHD), which causes the field to dissipate on a time $\tau \approx (\tau_r \tau_a)^{\frac{1}{2}}$ where τ_a is the Alfvén time scale. Such processes are called field reconnection (Petschek, 1964) or magnetic tearing (Furth et al. 1963) and they exhibit the proper behavior and a proper rate to explain a solar flare (Van Hoven 1976).

Figure 3 (Sturrock 1968), shows the coronal effects of such a reconnection or tearing in the two-ribbon flare example (v. Fig. 1). Outside of the reconnection point the ambient plasma is ejected into the outer corona, and inside it is accelerated onto the solar surface. This magnetic representation of a large flare is relatively well known and has been well analyzed previously. However, the question arises whether such a process can operate in different geometries such as that in a loop flare.

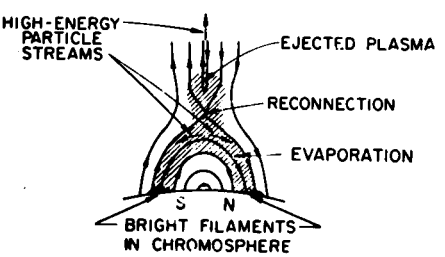

Fig. 3. The Preflare Field; Reconnection and its Consequences.

https://doi.org/10.1017/S1539299600004081 Published online by Cambridge University Press

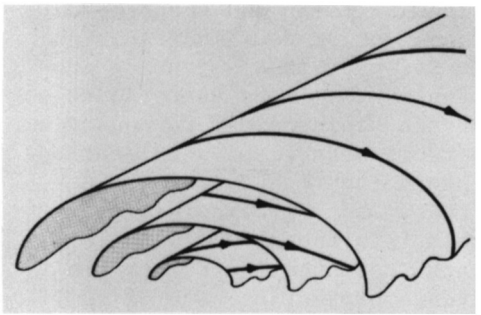

Fig. 4. Magnetic Field Shear.

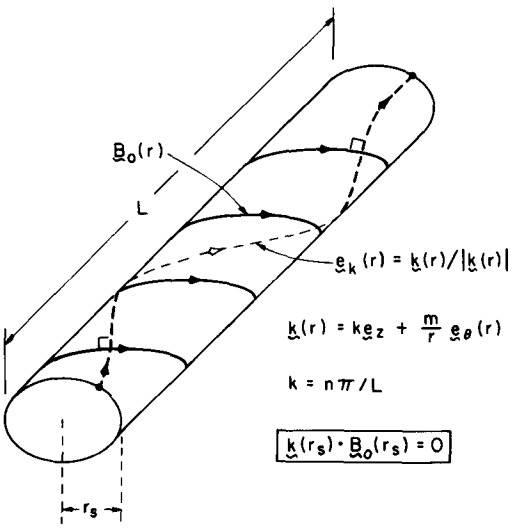

Fig. 5. The Singular Layer Showing the Boundary Resonance (dashed).

In the last several years, with great assistance from the toroidal confined-fusion program, this matter has become considerably clarified. Figure 4 shows an exaggerated view of a section of the preflare coronal loop, exhibiting (in particular) the magnetic shear or change in field direction with radius. Figure 5 isolates a particular magnetic surface in this loop in order to illustrate the concept of the singular layer. Unstable perturbations of the loop must, in some sense, resonate within the geometry of the loop, that is, within its periodic (poloidal) azimuthal angle and its finite (toroidal) length. Such boundary conditions establish a wavenumber-vector or wave-velocity direction which varies only slowly with radius. At the singular radius shown, this wavevector is directly across the magnetic field so that the field is only weakly disturbed by the perturbation. Near this stagnation layer the magnetic field is resistively decoupled from the fluid, breaking down the usual infinite-conductivity MHD frozen-in-field condition (Van Hoven 1979).

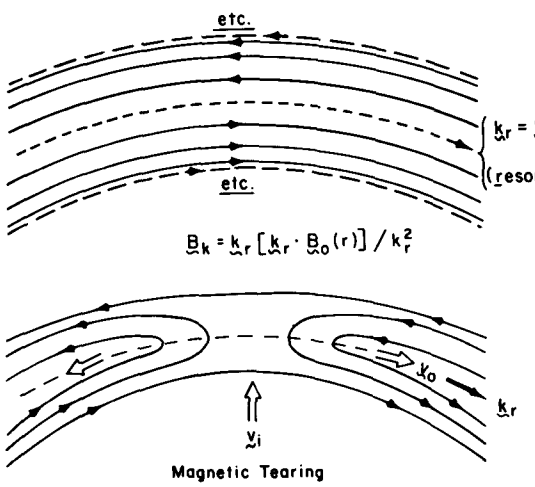

Fig. 6. Resistive Magnetic Tearing at the Singular Layer - Before and After.

If we look into the curvilinear plane of the wavevector ($\underset{\sim}{k}$, which is locally perpendicular to the principal field $\underset{\sim}{B}$) as shown in Fig. 6, we see first the residual parallel (to $\underset{\sim}{k}$) component of the magnetic field increasing

https://doi.org/10.1017/S1539299600004081 Published online by Cambridge University Press

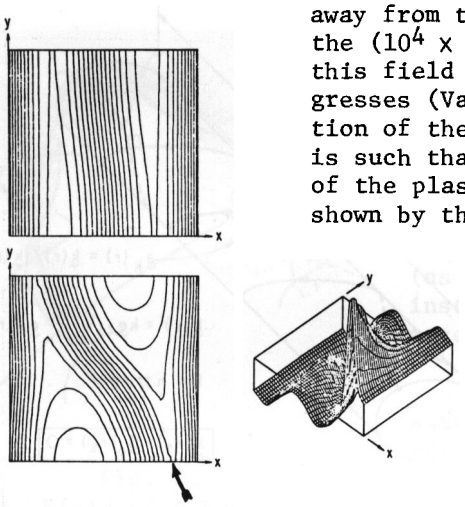

Fig. 7. Nonlinear Field Development in Tearing, and the Electric Field along B_z.

away from the singular layer and then, below, the (10^4 x vertically expanded) modification of this field as it is swept in and tearing progresses (Van Hoven 1979). The temporal relaxation of the magnetic field, after reconnection, is such that there is both Fermi acceleration of the plasma toward the right and left, as shown by the arrows, and a growing electric field into the slide (parallel to $\underset{\sim}{B}$) at the reconnection point. In this strange projection each of these directions $\underset{\sim}{k}$ and $\underset{\sim}{B}$, while mutually perpendicular, has a large component along the axis of the loop. Fluid particles are thus accelerated toward the foot points (Van Hoven 1979).

Nonlinear calculations of these accelerating fields have been made by a number of workers (Van Hoven 1976, 1979; Drake et al. 1978). Figure 7 shows a clear display of these effects due to the latter authors. In this example, which has two tearing layers, we see both the outward motion of the field lines giving rise to Fermi acceleration (on the lower left) and the very peaked, magnetically aligned, electric field (on the right) arising at the tearing point marked by the arrow.

In the solar flare context, magnetic reconnection or tearing grows in time and only certain aspects of the immediate energy deposition or release have been completely calculated so far (Van Hoven 1976, 1979). The amount of ambient heating is unknown because of the low emission measure and the difficulty of treating the effect of temperature changes on the resistivity, which in turn makes the process possible. The beam of accelerated particles, mainly electrons, increases in strength as the magnetic field sweeps in and is reconnected. It is known in other contexts that, if the resulting electron stream is too coherent or monoenergetic, it will excite electron plasma oscillations which will quickly grow and scatter and turbulently heat the beam until it becomes stable again. Thus, as represented in Fig. 3, one has an accelerated and heated beam moving away from the reconnection point which may or may not strongly interact with the ambient coronal plasma.

In a simple flare, as in a loop, the electron energy E is low enough so that there is strong collisional coupling to the ambient plasma ($dE/dt \propto n_a E^{-1/2}$). In this case the major effect is the heating of the loop by the confined beam. The local coronal temperature rises and there is energy transfer to the chromosphere through thermal conduction. This raises the chromospheric temperature to $\geq 10^4$ K and provides copious radiation in the extreme ultraviolet (EUV), white light and Hα.

https://doi.org/10.1017/S1539299600004081 Published online by Cambridge University Press

The high density chromospheric plasma then expands into the coronal loop so that, at the end, the loop density ($\sim 10^{11} cm^{-3}$) and temperature ($\sim 10^{7.3}$ K) have each risen by a factor of ten, providing the characteristic thermal soft X-ray and microwave emission of a simple flare (Svestka 1976).

A more complex case is that of the impulsive flare, which probably has more intrinsic interest in astrophysics. The temporal behavior of the radiations from such a flare are shown in Fig. 8, due to Kane (1974). We see a clear subdivision into a short impulsive phase and a longer thermal or decay phase.

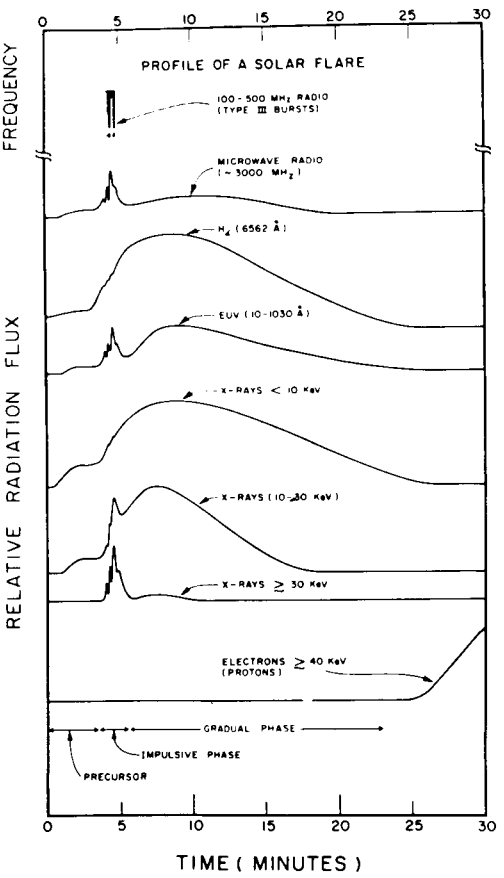

Fig. 8. The Impulsive and Gradual Phases of a Flare.

In an impulsive flare the initial electron beam has been accelerated to an energy of order 100 keV, well into the Coulomb-runaway range, and thus interacts weakly with the background plasma. Since > 10^{36} electrons (> 10^{29}ergs) are accelerated in 1 - 10 seconds, the self-magnetic field of such a beam (from Ampere's law) is sufficient to pinch or magnetically quench the beam. In order to circumvent this process, the unneutralized head of the beam generates a low-velocity return current in the much higher density ambient plasma (Ramaty et al. 1979). This return current then weakly heats the coronal plasma.

The majority of the subsequent effects are, however, due to the primary energetic electrons themselves. Their principal observable consequences are the emission of hard X-rays, due to bremsstrahlung, and of GHz microwaves, due to gyrosynchrotron radiation. The presently available X-ray data suffer from poor spatial, temporal, and energy resolution. Consequently, the source of the hard radiation is not well defined, nor is its thermal-vs-nonthermal character determined.

As shown in Fig. 9 (Kane et al. 1979), the microwaves originate high in the corona. Some of the hard X-rays are also emitted there, in the so-called thin-target region, wherein only a minority of the

https://doi.org/10.1017/S1539299600004081 Published online by Cambridge University Press

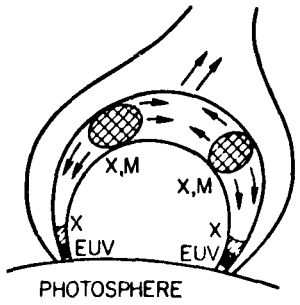

Fig. 9. The Hard X-ray and Microwave Sources of a Flare.

electrons' energy is lost. Further down, at the chromospheric end of the field lines, the electrons encounter the thick-target hard-x-ray source in which the majority of their energy is deposited. We will return below to the resulting thermal EUV radiation.

The radio effects of the primary electrons depend upon the magnetic field configuration. In particular their microwave gyrosychrotron emission, as compared with the hard X-rays, depends upon the pitch-angle ($\tilde{v}\cdot\tilde{B}$) distribution of the precipitated particles (Kane et al. 1979). There are also two mechanisms by which high-energy electrons get access to open field lines and thereby become sources for the emission of radially moving ($v \sim 0.5c$) Type-III radio bursts. Outside of the reconnection point electrons are accelerated directly into the outer corona, as shown schematically in Fig. 3; downwardly precipitating electrons are able to move, as a result of collisions in the high-density lower atmosphere, onto adjoining open field lines where they are expelled into the corona by magnetic mirroring action. Only one part per thousand of the original particles are believed to end up on open field lines and to cause Type-III bursts.

The most energetic of the accelerated electrons precipitate into the very high-density chromosphere ($n_e \sim 10^{13}$) and at that point dissipate the balance of their energy (Kane et al. 1979). At temperature levels less than $10^{4.8}$ K the density is high enough that the energy deposited can be radiated away. At higher altitudes the EUV emission ($\propto n_e^2$) is inadequate to dissipate the energy and the chromosphere is explosively unstable. The resulting shock wave, both on open and closed field lines, leads to drifting ($v \sim 10^8$cm/sec) Type-II radio bursts and to the further acceleration of both light and heavy particles, with results beyond the purview of this paper.

The energy deposited in the chromosphere (> 50% of the total) is sufficient to heat the ambient plasma so that it expands along the magnetic field lines and fills the flux tubes or loops which gave rise to the initial flare (Moore et al.

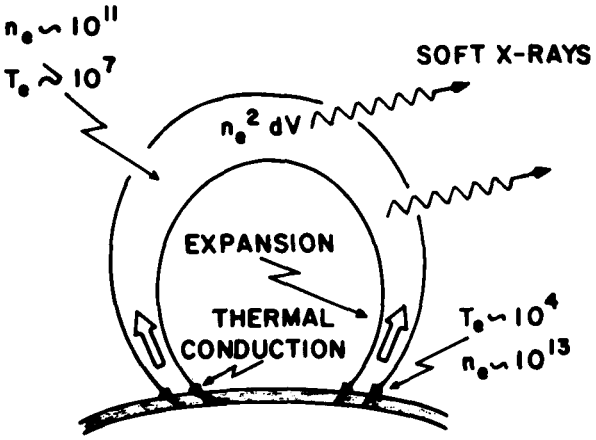

Fig. 10. The Late Phase of a Flare.

https://doi.org/10.1017/S1539299600004081 Published online by Cambridge University Press

1979). At this point the remaining energy has degraded to an elevated thermal level and the gradual decay phase of a flare begins, as shown in Fig. 10.

During the early part of this period the higher temperature corona loses its energy mainly through thermal conduction to the chromosphere, which causes continuing evaporation and expansion into the corona. At some point the coronal density becomes high enough that optically-thin soft-X-ray emission ($\propto n_e^2$) is sufficient to dissipate the remaining energy. With this balance between radiation and conduction, the thermal energy is steadily expended, bringing (over a period of an hour) the end of the solar flare excitation (Moore et al. 1979).

In the preceding pages, I have taken you though the chain of events leading from the initial energy release, through the thermalization phase to the final dissipation of a solar flare. This scheme is summarized in Fig. 11, for the case of an impulsive flare. I have concentrated on the central part of this diagram in which magnetic reconnection has as its principal effect the acceleration of electrons, with the immediate results shown by the double arrows, including the coronal reverse current.

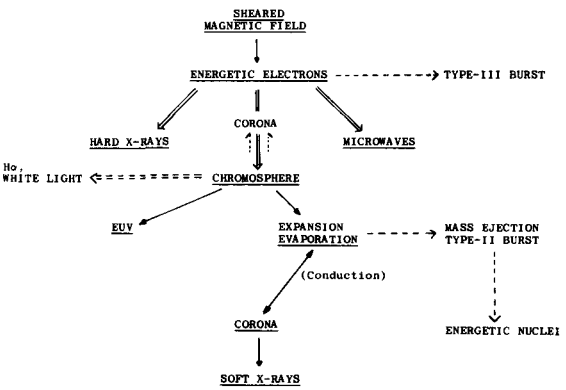

Fig. 11. The Energy Transformations and Observables of a Flare.

These electrons are mainly absorbed in the high-density target of the chromosphere, and the subsequent mass expansion and EUV radiation represent major flare outputs. The resulting conduction/evaporation equilibrium transfers much of the remaining excess energy back to the magnetic loops of the corona, where it finally emerges as soft-X-ray emission.

Many of the later stages of flare dissipation, observable in mass motions, EUV and soft X-rays, were measured in considerable detail during the Skylab and Orbiting Solar Observatory spaceflights. Although a number of puzzles remain, connected with the precise spatial and temporal relationships of the different temperature regimes during this period of the flare (Schmahl et al. 1978), our empirical understanding is relatively complete.

The situation is quite different with respect to the initial energy release and acceleration of the primary electrons. At the present time the hard X-rays and microwaves characteristic of this phase have been observed only with poor spatial and temporal resolution. This situation will improve considerably with the flight of the

https://doi.org/10.1017/S1539299600004081 Published online by Cambridge University Press

Solar Maximum Mission which is to be launched early next year. The great strength of the instrument package of this spacecraft is in its initial impulsive-phase high-energy spectral diagnostics, ranging from soft X-rays through hard X-rays to gamma rays. It is our hope that the data obtained by the SMM spacecraft, and the other coordinated observations (including high-resolution radio measurements) of the current Solar Maximum Year, will specify more completely some of the complex of impulsive interactions which I have described in this presentation.

The research contributing to this review was supported in part by the Solar Physics Branch of the National Aeronautics and Space Administration under grant NSG-7375, the Atmospheric Sciences Section of the National Science Foundation under grant ATM77-09581 A01, and by the Graduate Council of the University of California at Irvine.

Much of the point of view and specific information contained in this paper resulted from the author's participation in the Skylab Workshop on Solar Flares, sponsored by NASA and the National Center for Atmospheric Research.

REFERENCES

Drake, J. F., Pritchett, P. L., and Lee, Y. C., 1978. University of California, Los Angeles, Plasma Physics Group, Report No. PPG-341.
Furth, H. P., Killeen, J., and Rosenbluth, M. N., 1963. Phys. Fluids, 6, 459.
Kane, S. R., 1974. IAU Symp. 57, p. 105.
Kane, S. R., et al., 1979. "Impulsive Phase of Solar Flares," in Solar Flares (Sturrock 1979).
Moore, R. L., et al., 1979. "The Thermal X-Ray Plasma," in Solar Flares (Sturrock 1979).
Petschek, H. E., 1964. AAS-NASA Symposium on the Physics of Solar Flares, NASA, SP-50, p. 425.
Ramaty, R., et al., 1979. "Energetic Particles in Solar Flares," in Solar Flares (Sturrock 1979).
Schmahl, E. J., Solodyna, C. V., Smith, J. B., and Cheng, C.-C., 1978. Solar Phys., 60, 323.
Sturrock, P. A., 1974. Flare-Related Magnetic Field Dynamics, High Altitude Observatory (Boulder, Colorado), p. 187.
Sturrock, P. A. (ed.), 1979. Solar Flares, Proceedings of the Second Skylab Workshop, Univ. of Colorado (Boulder).
Svestka, Z., 1976. Solar Flares, Reidel (Dordrecht, Holland).
Van Hoven, G., 1976. Solar Phys., 49, 95.
Van Hoven, G., 1979. Astrophys. J., 232, 572.
Van Hoven, G., et al., 1979. "The Preflare State," in Solar Flares (Sturrock 1979).